Nanopackaging:

Nanotechnologies in Microelectronics Packaging

James E. Morris
Department of Electrical & Computer Engineering,
Portland State University, Portland, Oregon, USA
j.e.morris@ieee.org

Portland State UNIVERSITY

Nanoelectronics & Packaging Lab

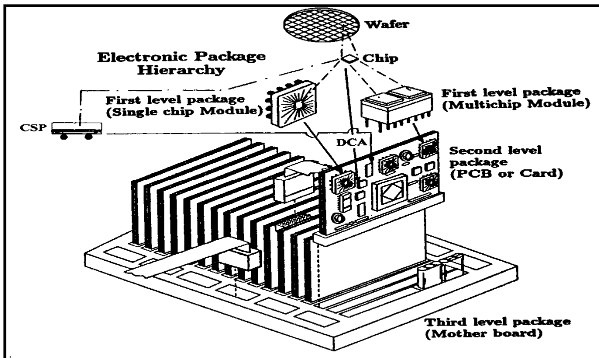

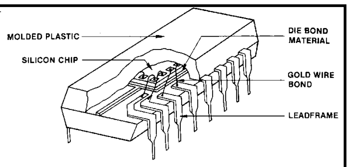

FIGURE 1-12. Cutaway view of a postmolded plastic package in the configuration of a dual-line package (DIP).

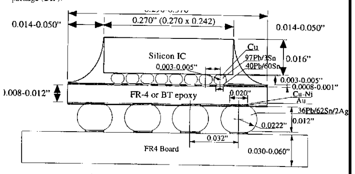

Figure 1: Schematic of a SLICC package.

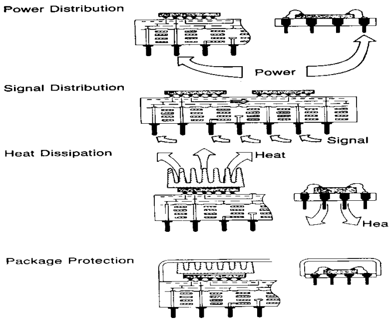

Figure 1-1. Four Major Functions of the Package. + Mechanical support.

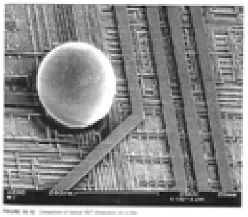

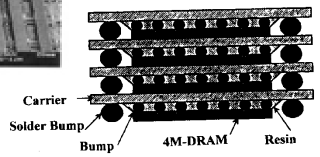

Figure 1.11 NEC's 3-D stack-up chip scale package (CSP) for memory devices.

Nanopackaging

Nanoelectronics & Packaging Lab

- Primary current issues in Microelectronics Packaging
  - Embedded passives
  - Thermal dissipation
  - 3D integration
- Nanotechnologies in Microelectronics Packaging
  - Nanoparticles
  - Carbon nanotubes
  - Nanoparticles & CNTs in ECAs
  - Nanowires, nanospring contacts

Portland State UNIVERSITY

11/13/2009

Nanoparticle inclusion in epoxy: $AgNO_3$

[Wong et al, ECTC'06] [Jiang/Moon/Wong APM'05] [Pothukuchi/Li/Wong ECTC'04]

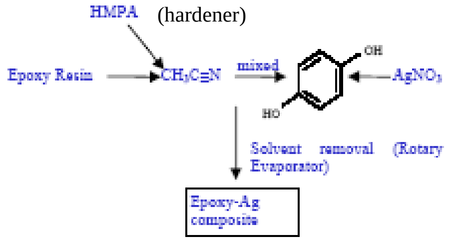

Fig. 4 Schematic illustration of the preparation of the *in-situ* conductive adhesives

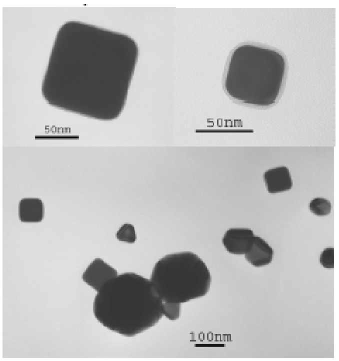

Figure.1 Silver nanocubes as obtained by the procedure detailed.

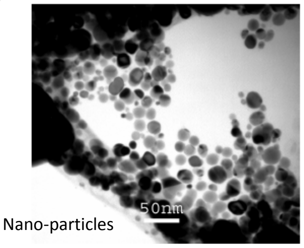

Fig. 10 Silver nanoparticles *in-situ* formed in the cycloalophatic epoxy matrix in the presence of HMPA

Surface treatments to avoid agglomeration

Figure 1. Scheme of surface modification for nano-size filler

Nanoparticle Properties (High surface/volume ratio→**catalysts, etc)**

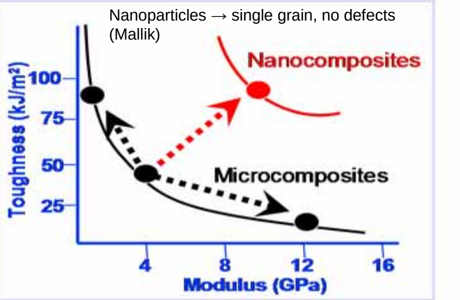

Nanoparticles → single grain, no defects (Mallik)

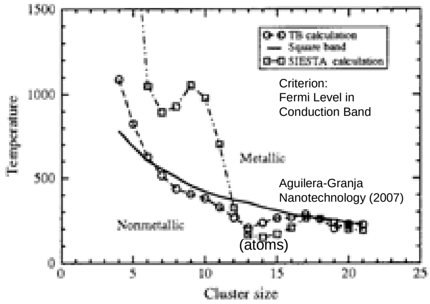

Criterion:
Fermi Level in
Conduction Band

Aguilera-Granja
Nanotechnology (2007)

(atoms)

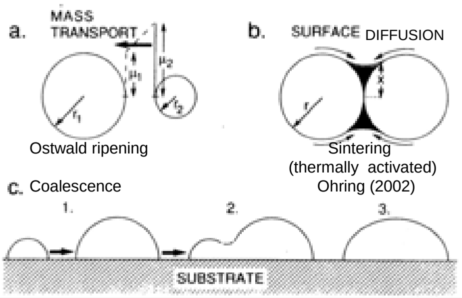

DIFFUSION

Ostwald ripening

Sintering
(thermally activated)
Ohring (2002)

Coalescence

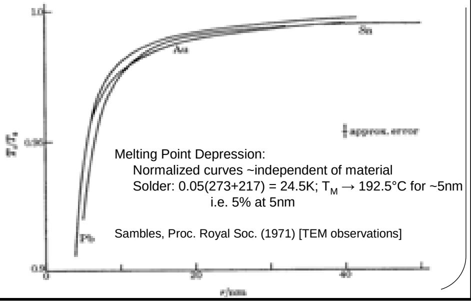

Melting Point Depression:
Normalized curves ~independent of material
Solder: 0.05(273+217) = 24.5K; T_M → 192.5°C for ~5nm
i.e. 5% at 5nm

Sambles, Proc. Royal Soc. (1971) [TEM observations]

Melting Point Depression in Nanoparticle No-Pb Solders

(Johan Liu et al, EPTC 2008)

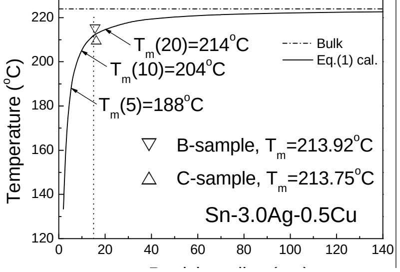

$T_m(20)=214^oC$

$T_m(10)=204^oC$

$T_m(5)=188^oC$

▽ B-sample, $T_m=213.92^oC$

△ C-sample, $T_m=213.75^oC$

Sn-3.0Ag-0.5Cu

(Hongjin Jiang et al, ECTC'07)
[found by DSC]

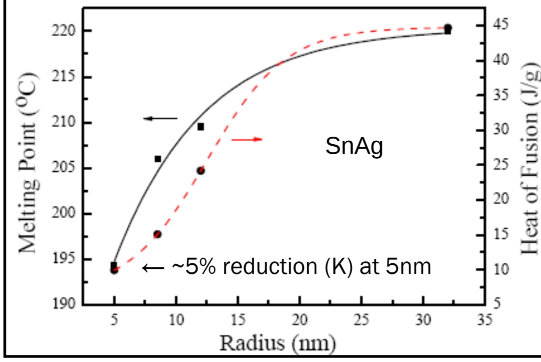

SnAg

← ~5% reduction (K) at 5nm

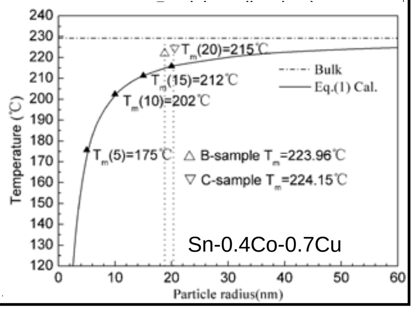

Sn-0.4Co-0.7Cu

Embedded PWB passives (Das et al, ECTC 2009, 591-598)

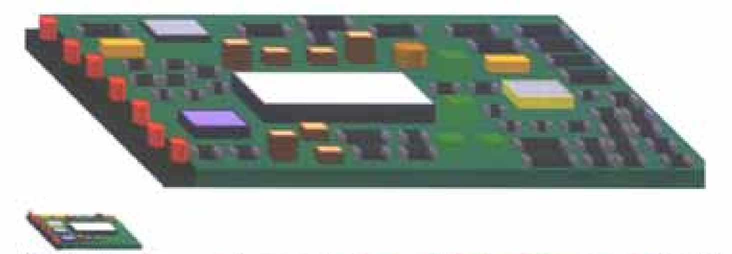

Figure 11: PWB vs. SiP

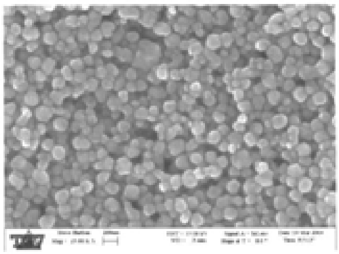

Figure 3: Larger area SEM images of RC3 nanocomposites.

BaTiO$_3$
Nanoparticles

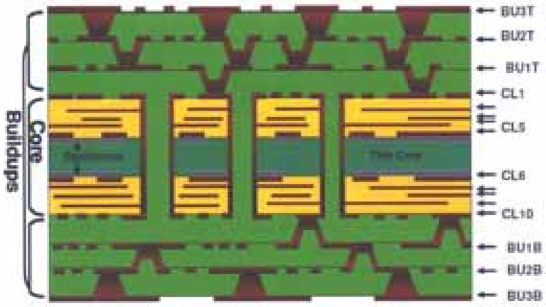

Figure 2: System in a Package (SiP): 3-10-3 cross section using resin coated copper capacitive (RC3) materials. Substrate cross section has resistance layers in the middle.

High-*k* Ag nanocomposites

Ag nanoparticles from AgNO$_3$

Coulomb blockade effect reduces leakage/loss?

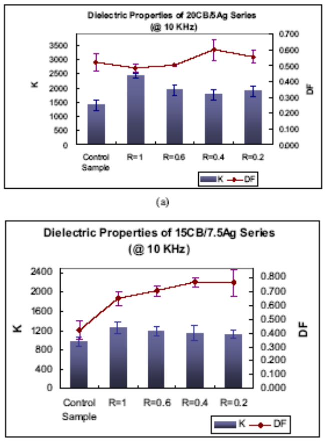

(b)

Fig. 9. K and Df values of (a) 20CB/5Ag series and (b) 15CB/7.5Ag series Ag/CB/epoxy composites with various loading of a surfactant (R= [surfactant]/[AgNO$_3$])

[Lu/Moon/Xu/Wong, APM'05]

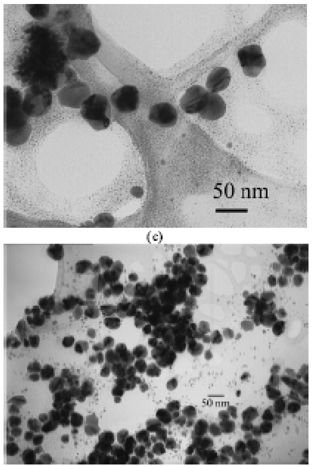

(d)

Fig. 3. TEM micrograph of Ag/epoxy composite in the presence of a surfactant with (a) [surfactant]/[AgNO$_3$] ratio R = 1, (b) R = 0.6, (c) R = 0.4 and (d) R = 0.2.

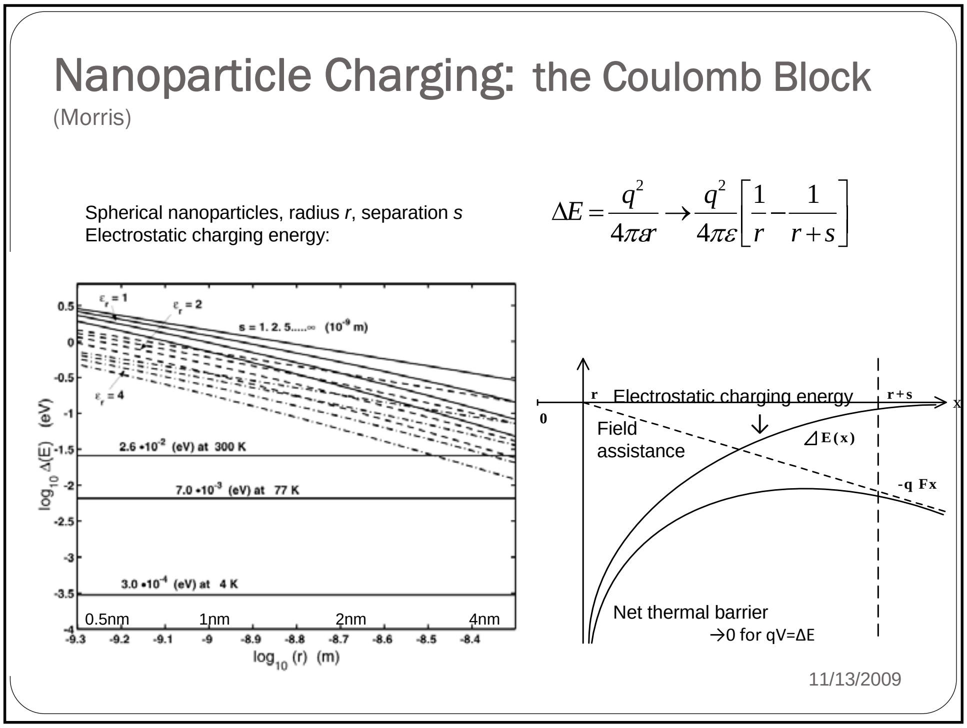

Nanoparticle Charging: the Coulomb Block

(Morris)

Spherical nanoparticles, radius *r*, separation *s*
Electrostatic charging energy:

$$\Delta E = \frac{q^2}{4\pi\varepsilon r} \rightarrow \frac{q^2}{4\pi\varepsilon}\left[\frac{1}{r} - \frac{1}{r+s}\right]$$

11/13/2009

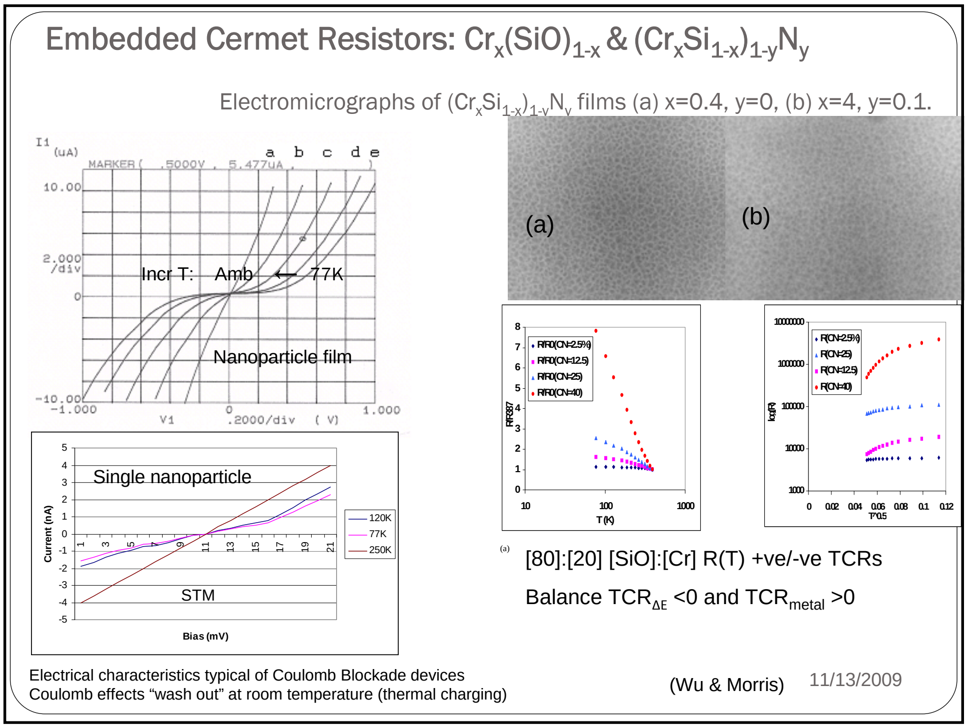

Embedded Cermet Resistors: $Cr_x(SiO)_{1-x}$ & $(Cr_xSi_{1-x})_{1-y}N_y$

Electromicrographs of $(Cr_xSi_{1-x})_{1-y}N_y$ films (a) x=0.4, y=0, (b) x=4, y=0.1.

[80]:[20] [SiO]:[Cr] R(T) +ve/-ve TCRs

Balance $TCR_{\Delta E}$ <0 and TCR_{metal} >0

Electrical characteristics typical of Coulomb Blockade devices
Coulomb effects “wash out” at room temperature (thermal charging)

(Wu & Morris)

11/13/2009

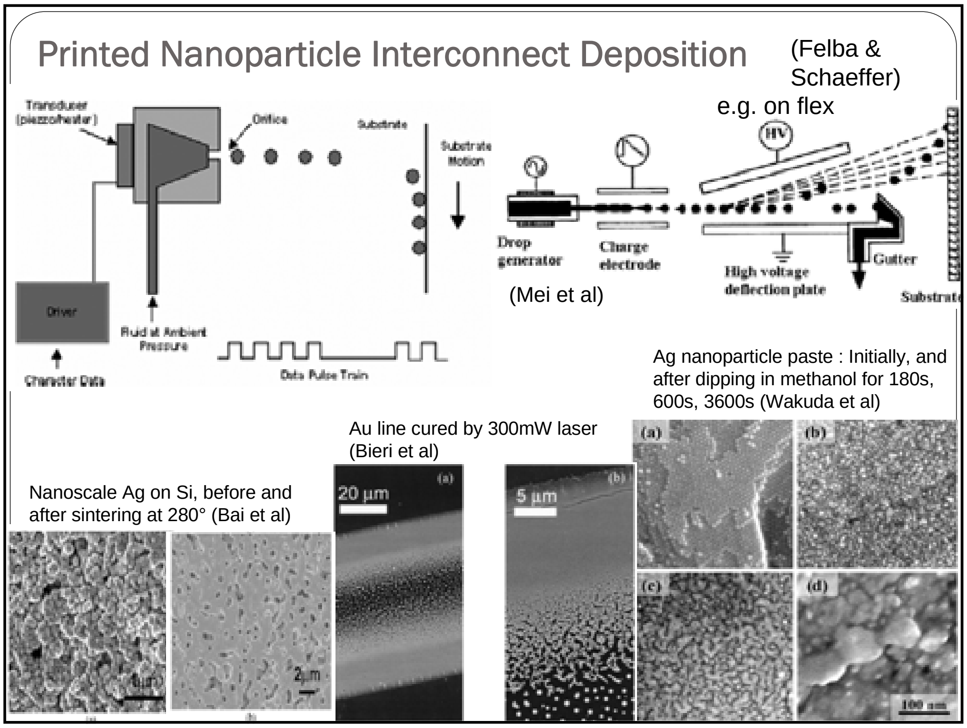

Printed Nanoparticle Interconnect Deposition

(Felba & Schaeffer)

e.g. on flex

(Mei et al)

Ag nanoparticle paste : Initially, and after dipping in methanol for 180s, 600s, 3600s (Wakuda et al)

Au line cured by 300mW laser (Bieri et al)

Nanoscale Ag on Si, before and after sintering at 280° (Bai et al)

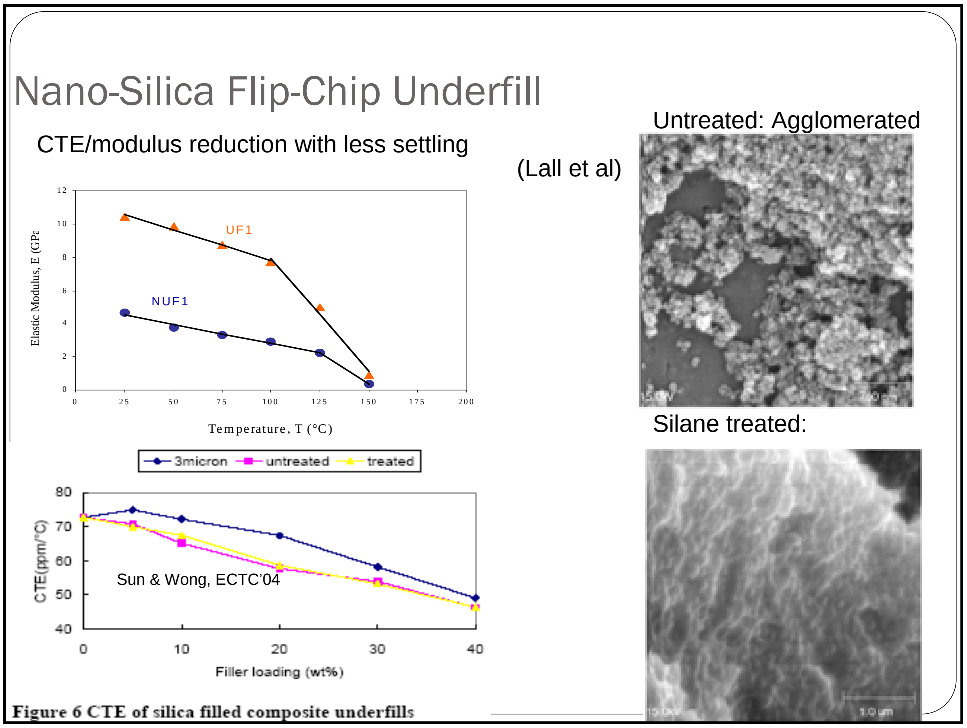

Nano-Silica Flip-Chip Underfill

CTE/modulus reduction with less settling

(Lall et al)

Untreated: Agglomerated

Silane treated:

Sun & Wong, ECTC'04

Figure 6 CTE of silica filled composite underfills

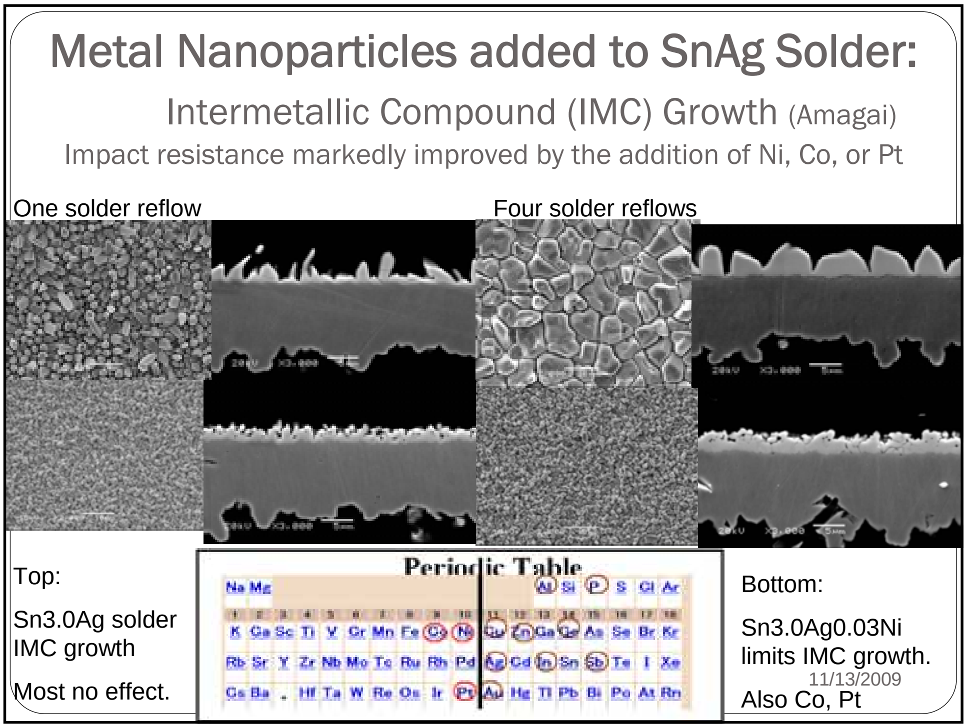

Metal Nanoparticles added to SnAg Solder:

Intermetallic Compound (IMC) Growth (Amagai)

Impact resistance markedly improved by the addition of Ni, Co, or Pt

One solder reflow

Four solder reflows

Top:

Sn3.0Ag solder IMC growth

Most no effect.

Bottom:

Sn3.0Ag0.03Ni limits IMC growth.

11/13/2009

Also Co, Pt

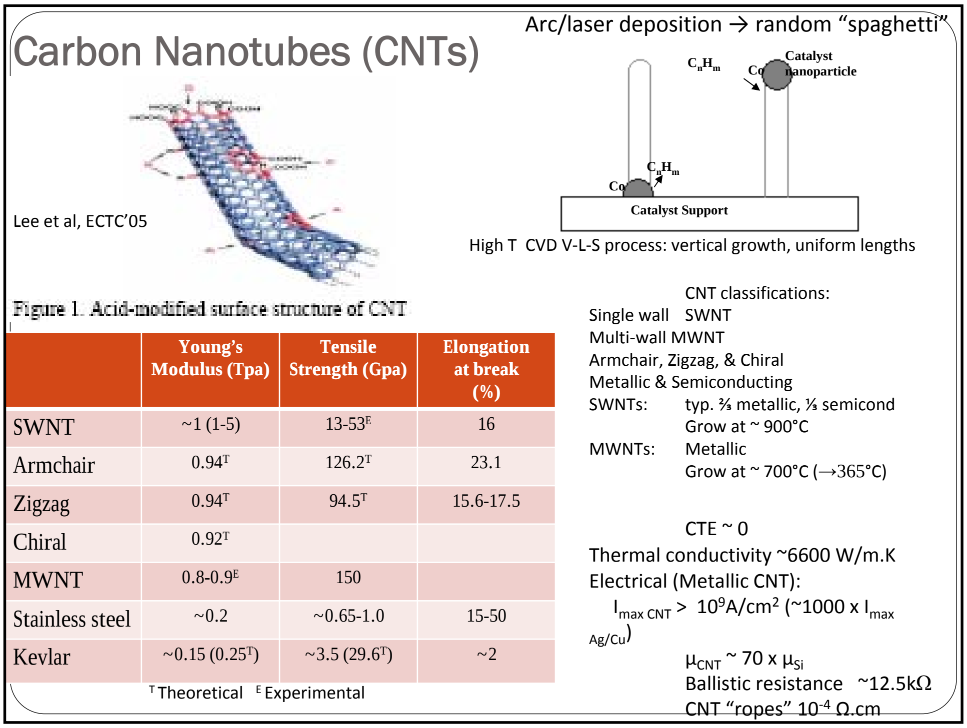

Carbon Nanotubes (CNTs)

Lee et al, ECTC'05

Figure 1. Acid-modified surface structure of CNT

Arc/laser deposition → random "spaghetti"

High T CVD V-L-S process: vertical growth, uniform lengths

	Young's Modulus (Tpa)	Tensile Strength (Gpa)	Elongation at break (%)
SWNT	~1 (1-5)	13-53^E	16
Armchair	0.94^T	126.2^T	23.1
Zigzag	0.94^T	94.5^T	15.6-17.5
Chiral	0.92^T		
MWNT	0.8-0.9^E	150	
Stainless steel	~0.2	~0.65-1.0	15-50
Kevlar	~0.15 (0.25^T)	~3.5 (29.6^T)	~2

^{T} Theoretical ^{E} Experimental

CNT classifications:

Single wall	SWNT
Multi-wall	MWNT

Armchair, Zigzag, & Chiral

Metallic & Semiconducting

SWNTs:	typ. ⅔ metallic, ⅓ semicond Grow at ~ 900°C
MWNTs:	Metallic Grow at ~ 700°C (→365°C)

CTE ~ 0

Thermal conductivity ~6600 W/m.K

Electrical (Metallic CNT):

$I_{max\ CNT} > 10^9$A/cm^2 (~1000 x $I_{max\ Ag/Cu}$)

$\mu_{CNT} \sim 70 \times \mu_{Si}$

Ballistic resistance ~12.5kΩ

CNT "ropes" 10^{-4} Ω.cm

EMC Shielding

MWCNTs (Cheng et al)

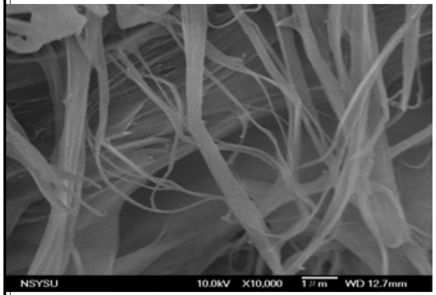

Oh et al, Nanotechnology, 19 (2008) 495602

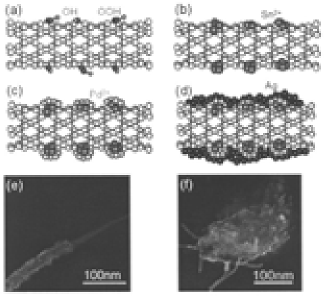

Figure 3. A schematic of electroless silver plating on carbon nanotubes: (a) carboxyl group functionalized nanotubes by the acid treatment process, (b) Sn^{2+} sensitization, (c) preactivation of nanotubes by Pd^{2+}, (d) electroless silver plating, (e) SEM image of the electroless-plated silver on a single MWNT, (f) a lump of silver sandwiching multiple MWNTs.

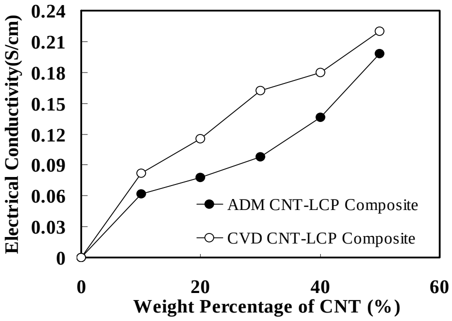

Shielding Improvement (Ionic Liquid) at low CNT content
(Jin-Chen Chiu, ECTC'08)

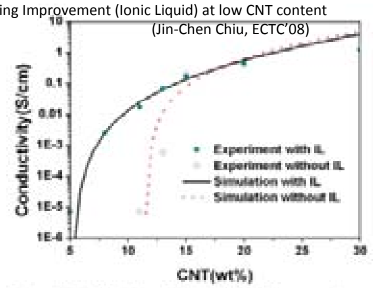

Figure 7 Conductivity of the MWCNT/PI composite at various weight percentage of MWCNT

Open-ended CNTs for electrical interconnect

Xiao et al, ECTC 2009, 1811-1815

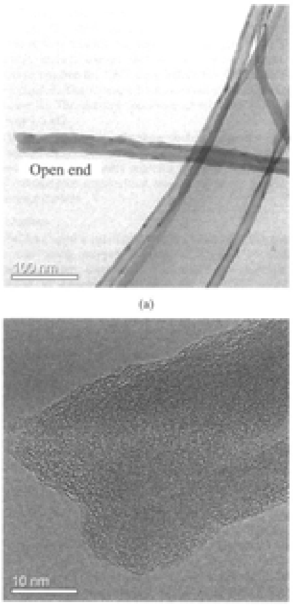

(a)

(b)

Fi 8: (a) TEM micrograph of an open-ended CNT tip, (b)
c view of (a).

S al removal of CNT caps

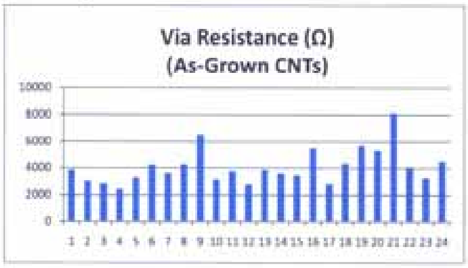

Figure 9: Via resistance with as-grown CNTs.

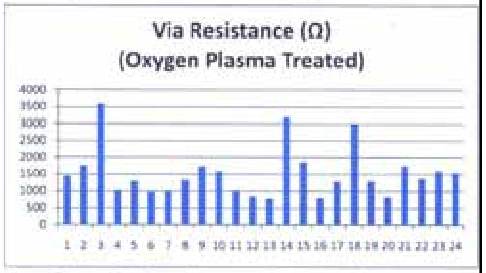

Figure 10: Via resistance with truncated CNTs.

CNT Interconnect

(Naaemi, Huang, & Meindl, ECTC 2007)
(Banerjee, Li, Srivastava NANO 2008)

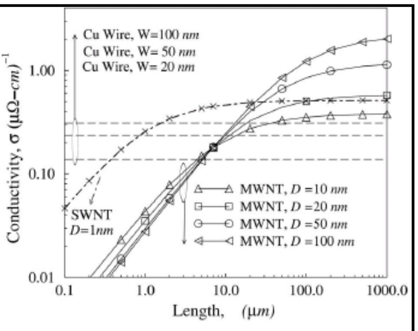

Figure 3: Conductivity of MWCNs with various diameters and bundles of densely packed SWCNs versus length. SWCNs are assumed to be 1nm in diameter and have random chiralities and a 1μm mean free path.

TABLE I. Comparison of properties among Cu, SWCNT, and MWCNT.

	Cu	SWNCT	MWCNT
Max. current density (A/cm^2)	<1x10^7	>1x10^9 [5]	
Thermal conductivity (W/mK)	385	5800 [6]	3000 [7]
Mean free path (nm) @ $300K$	40	>1000 [8]	>25000 [9]*

* MFP of MWCNTs depends on their diameters. The value shown here is fo
the MWCNT with outmost shell diameter of 100 *nm*.

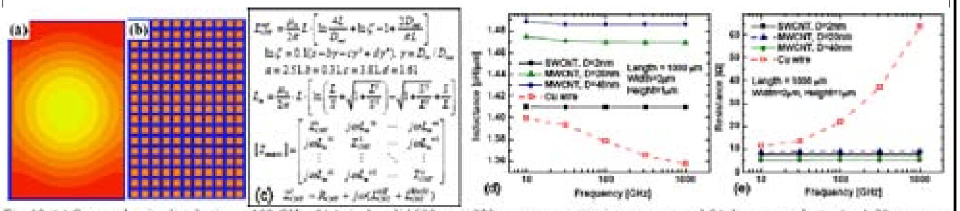

Fig. 10. (a) Current density distribution at 100 *GHz* of (a) single solid 500 *nm* × 320 *nm* cross- section interconnect, and (b) discrete conductor (each 20 *nm* square cross-section, 10 *nm* interval) using electromagnetic field solver Maxwell [33]. Both of them have identical "equivalent conductivity", and identical current density is applied. Color coding in the two cases is identical. (c) Equations of inductance model. L_{CNT}^{self} and L_m are magnetic self- and mutual- inductance of each CNT. S is the distance between CNTs, Z_{matrix} is the impedance matrix of CNT bundle. Effective total (d) inductance, and (e) resistance of SWCNT and MWCNT bundles, and Cu interconnects as a function of frequency for the same dimension.

CNTs in TSVs

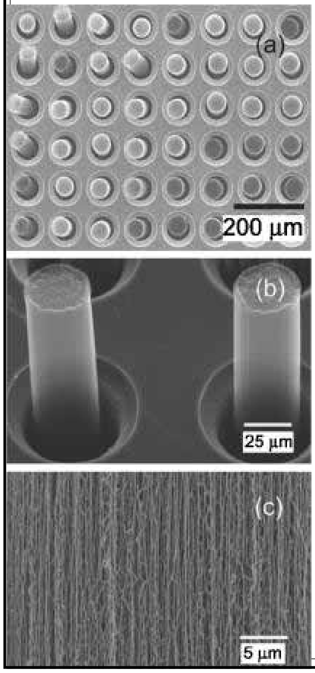

←Xu et al, Appl Phys Lett (2007)

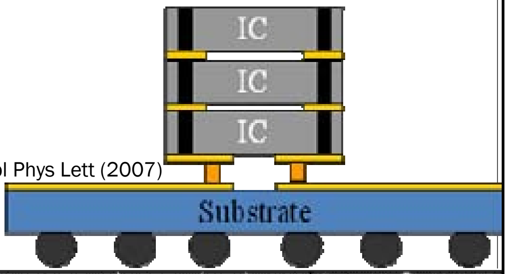

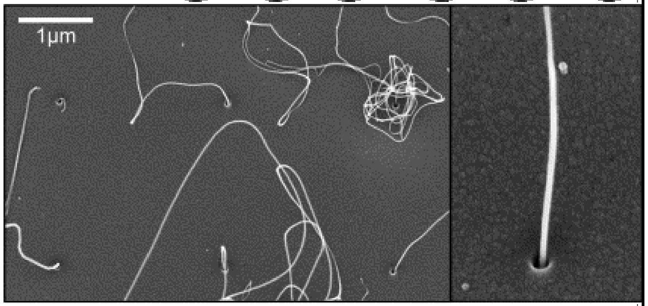

15nm MWNTs in 35nm vias
Graham et al, Diamond & Related materials (2004)

11/13/2009

CNT inductors

(Mousa, Kim, Flicker, Ready, ECTC 2009, 497-501)

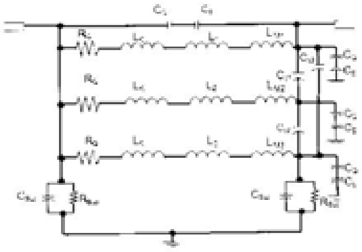

Fig 4. Equivalent Circuit Model of a Two-Port MWCNT Inductor on an FR-4 or Ceramic Substrate.

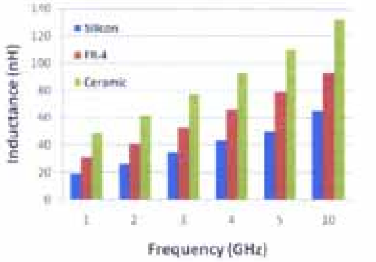

Fig. 8. Inductance Values for Carbon Nanotube Inductors on Silicon, FR-4, and Ceramic Substrates.

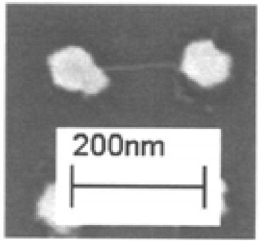

Fig. 6. Approximately 100nm long Single-Wall Carbon ube Interconnect that Shows Good Alignment Between Two 30 nm Electron Beam Nickel Islands.

Table 1. Carbon Nanotube-Based Inductor Quality Factors for Silicon, FR-4, and Ceramic Substrates.

Freq (GHz)	Q on Silicon	Q on FR-4	Q on Ceramic
1	162	1872	3671
2	189	2751	5102
3	297	3812	7766
4	372	4899	9101
5	440	5601	10990
10	1469	15010	23129
20	2510	20109	49925

SWCNT Effects on 63Sn-37Pb & Sn-3.8Ag-0.7Cu Solders

(Kumar et al)

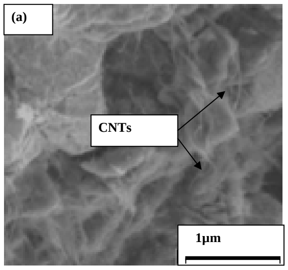

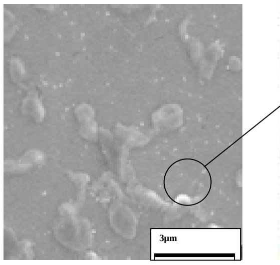

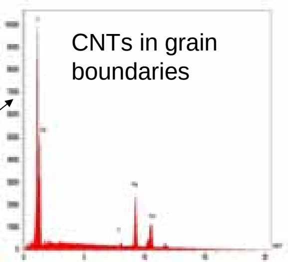

CNTs in grain boundaries

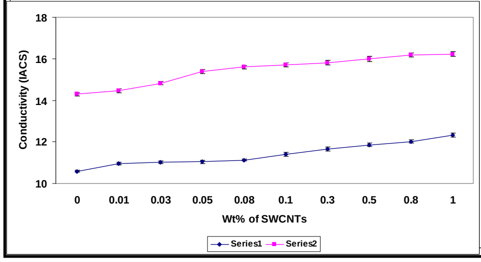

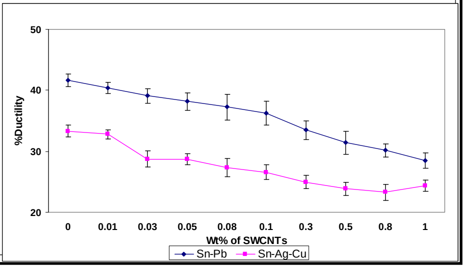

Mechanical Effects (Yamamoto, Nanotechweb.org)

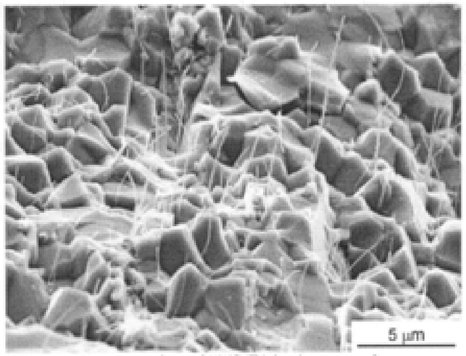

Fracture surface of MWCNT/alumina composite

Acid etch:
- Aids dispersion
- Increased interfacial friction
- Better than smooth CNTs

CRACK BRIDGING

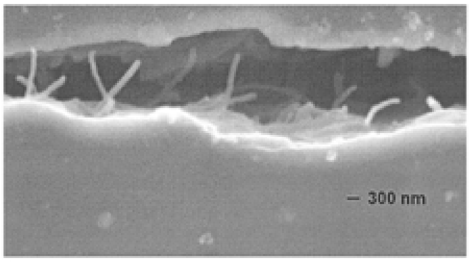

SEM image of a fatigue crack being bridged by carbon nanotube fibres. (Image credit: Rensselaer Polytechnic Institute)

0.9 vol % acid-etched CNTs:
- +27% bending strength
- +25% fracture toughness

Electromigration

(Yang Chai et al ECTC'08)

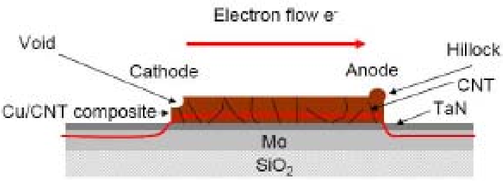

Figure 1: Schematic diagram of *Blech-Kinsbron* segment cross-section, showing shunting of current out of the bottom conductor into the top Cu/CNT stripe, depletion of the cathode, and mass accumulation at the anode.

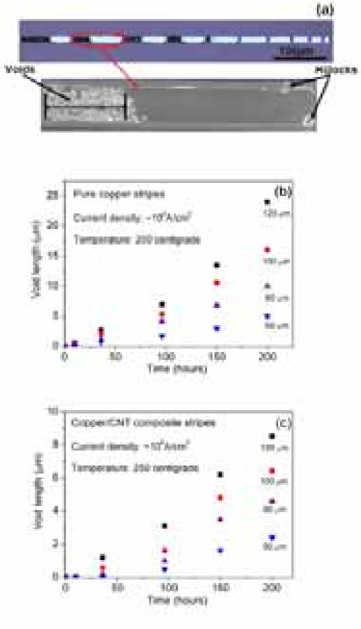

Figure 10: (a) Photograph of pure copper stripes with different lengths after EM testing, and SEM image of one of the segments; Plots of void growth length as a function of the stressing time for short (b) Cu and (c) Cu/CNT composite stripes.

CNTs inhibit void growth

CNT Contact Bumps

(Liu & Wang)

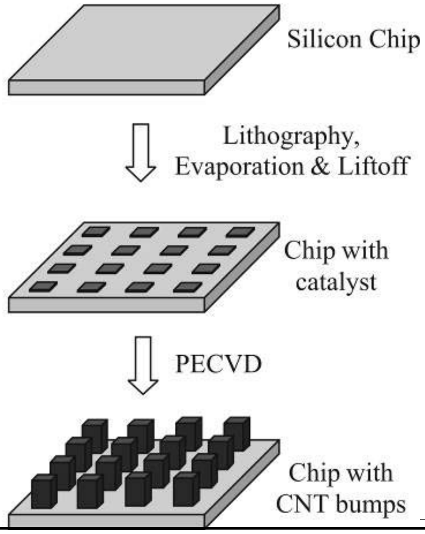

Silicon Chip

Lithography,
Evaporation & Liftoff

Chip with
catalyst

PECVD

Chip with
CNT bumps

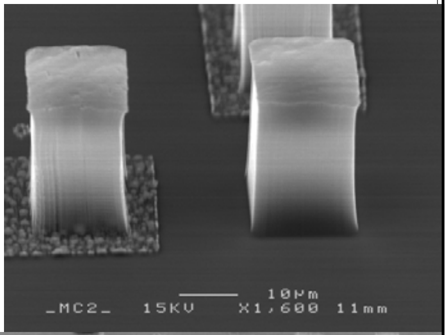

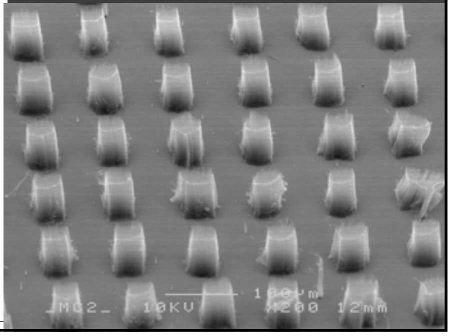

Placement of Aligned CNTs for Packaging

(Kyoung-Sik Moon, ECTC'08; Zhu et al, ECTC'06; Soga et al, ECTC'08)

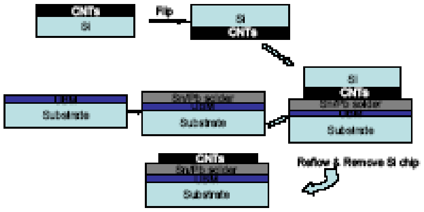

Figure 6. Schematic diagram of "CNT transfer technology". UBM: under bump metallization. See the text for detailed explanations.

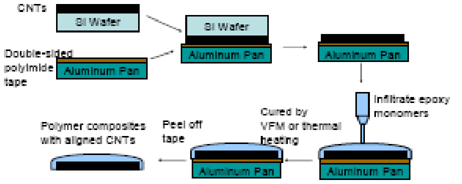

Figure 2. Schematic of the CNT-polymer composite preparation process using double-sided polyimide tape as a transferring layer.

CNT Growth on Si: Localized heating (Ting Xu et al, ECTC'08) ΔT~400°C


(a)

(b)

Figure 2. Optical image of the fabricated micro-heater. (a) micro-heater array; (b) detailed view of an individual heater.

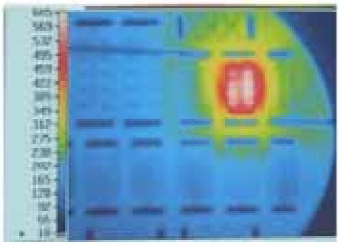

Figure 3. Temperature distribution on the wafer after the D voltage was supplied to the micro-heaters.

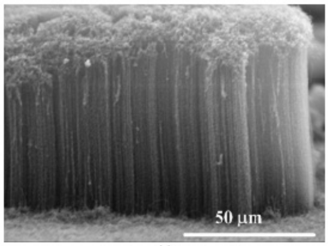

CNT Thermal Interface (Zhang et al, ECTC'06)

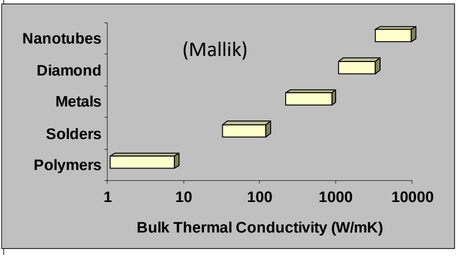

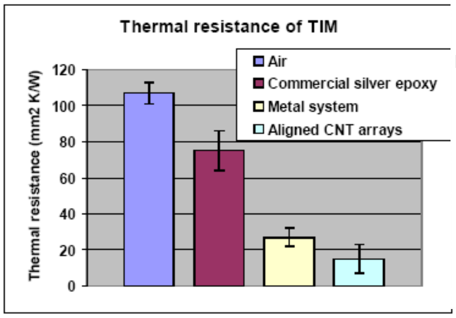

Fig.8 Measured thermal resistance of different TIM

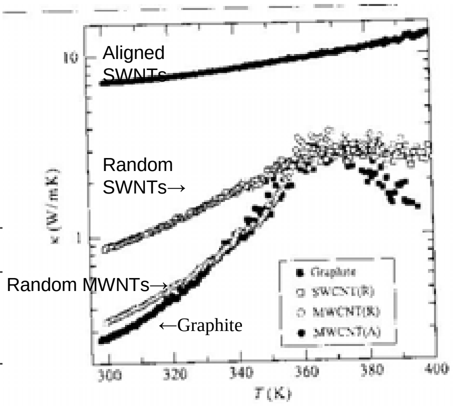

Figure 5. A semi-log plot of the derived effective thermal conductivity of bulk graphite powder (solid squares), random thin films of SWCNT (open squares) and MWCNT (open circles), as well as aligned MWCNT (solid circles) as function of temperature from 300 to 400 K.

Pradham et al,
Nanotechnology, 20 (2009) 245705

CNT Heat Sink

(Liu & Wang)

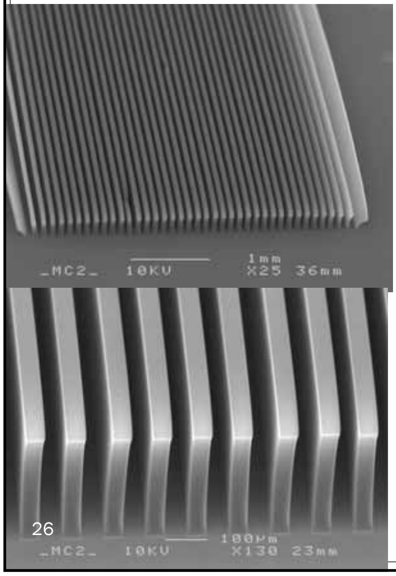

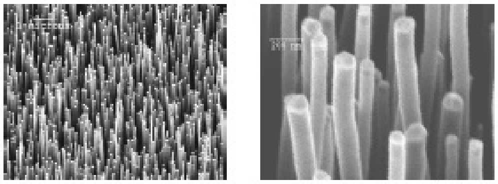

Fig. 1. SEM image of MWCNT from plasma deposition. The scale bar on the left is 1 micron and the one on the right is 200 nm.

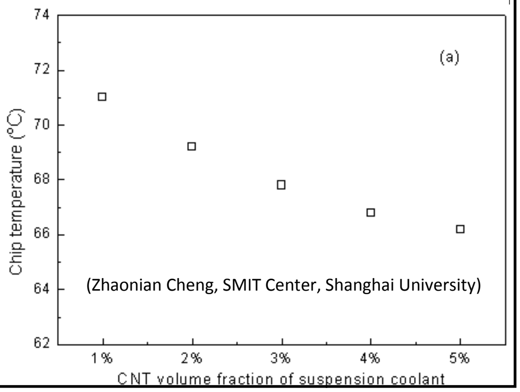

(Zhaonian Cheng, SMIT Center, Shanghai University)

Nanoparticles in Isotropic Conductive Adhesives (ICAs)

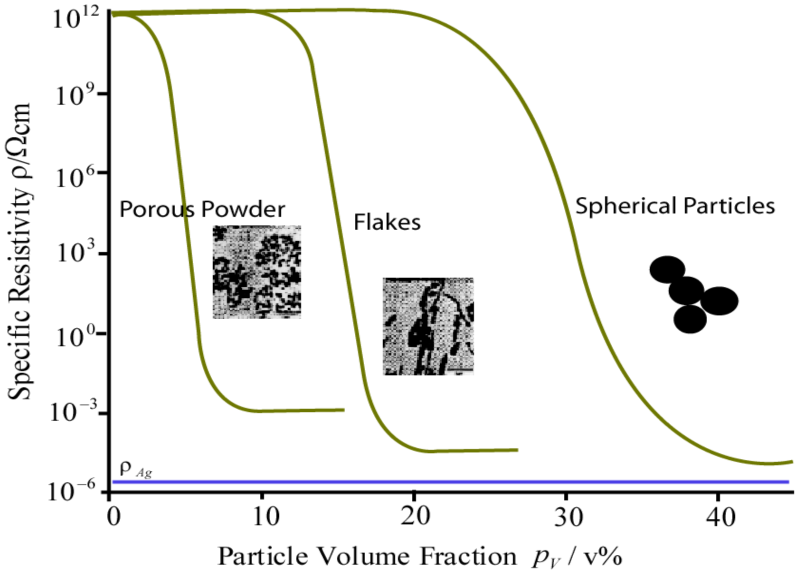

Ag nanoparticles added to Ag-flake ICAs

Fan/Su/Qu/Wong [ECTC 2004]
[Wong et al, ECTC'06]

- 80% Ag + nanoparticles: no effect
- 70% Ag + nanoparticles: percolation threshold
- Ag more effective as flakes
- Until sintering!

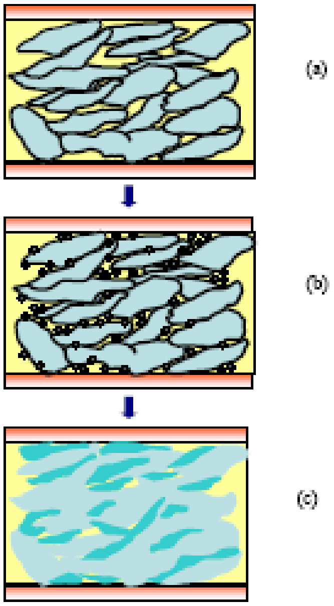

Figure 1. Schematic of particles and flakes between the metal and pads. (a) is conductive adhesives with silver flakes as fillers; (b) is conductive adhesives with both flakes and nanoparticles as fillers; (c) is conductive adhesives with sintered particles among flakes as fillers.

Nano-particle sintering

[Wong et al, ECTC ’04 & ’06]

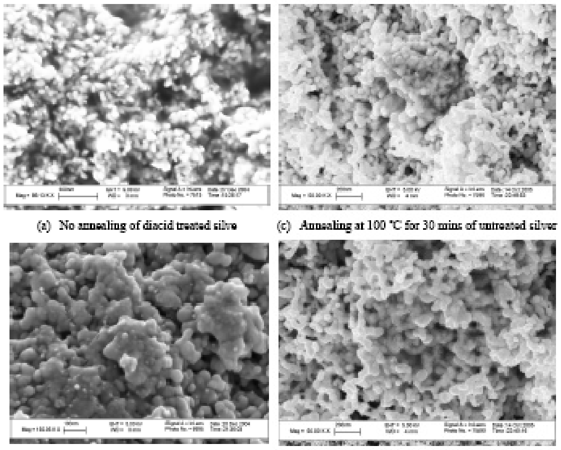
(a) No annealing of diacid treated silve

(c) Annealing at 100 °C for 30 mins of untreated silver

(b) Annealing at 150 °C for 30 mins of diacid treated silver

(d) Annealing at 100 °C for 30 mins of diacid treated silver

Figure 4. Comparison of the morphologies of silver nanoparticles without treatment and treated by diacids before and after annealing at 100°C and 150°C for 30 mins.

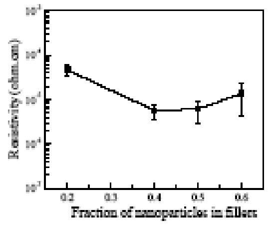

Figure 5. The bulk resistivity of the isotropic conductive adhesives with 5wt% diacids as surfactants

Surfactants: 5% diacids

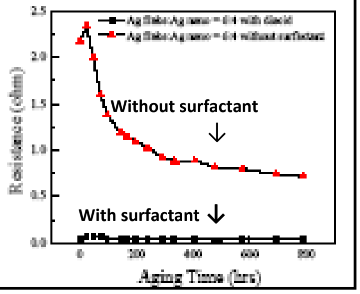

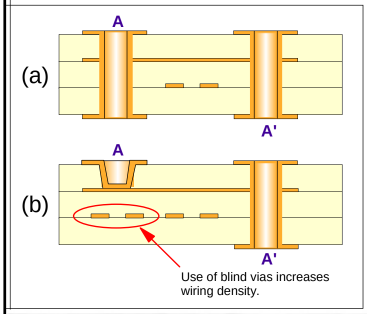

Use of blind vias increases wiring density.

Das & Egitto

ICA Microvia Fill (PWB)

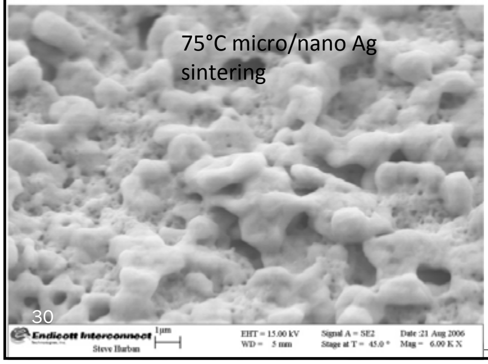
75°C micro/nano Ag sintering

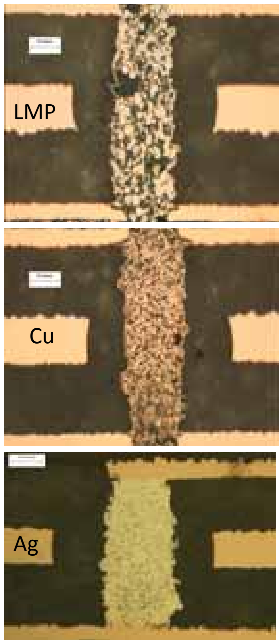

Ag Nanowire Anisotropic Conductive Film (ACF) (Au seed, Co alignment)

[Lin et al, ECTC'05]

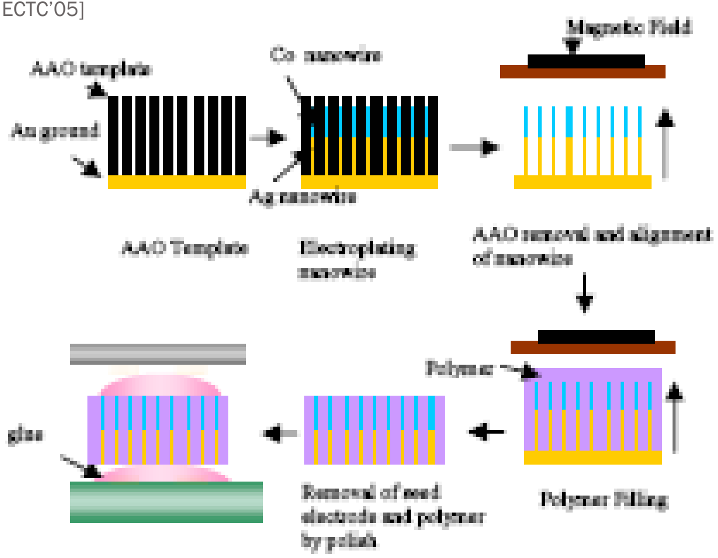

Fig. 1 Process Flow of Nanowire Conductive Film

Ni Nanowire Contacts

[IEEE Trans CPT (2008)]

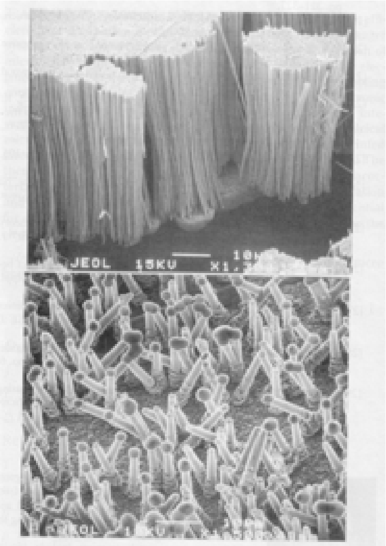

Fig. 13. Scanning electron microscope (SEM) Images of nickel nanowires. 0.2 × 60 μm nickel nanowires (top) are fabricated from an alumina filter and 2.0 × 20 μm nickel nanowires with a sphere at the tip (bottom) are fabricated by replating.

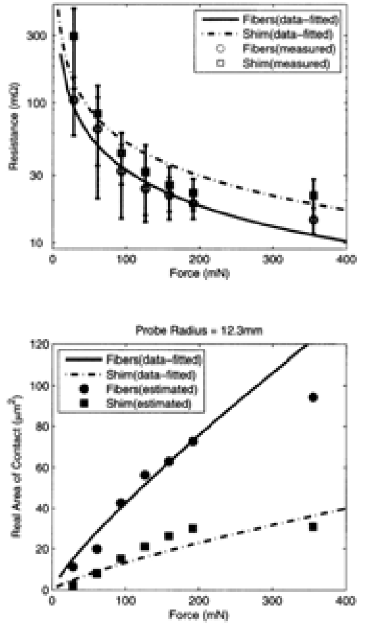

Fig. 11. Resistance of an array of 0.2 × 10 μm nickel nanowires and the resistance of a nickel shim were measured by a micro-ohmmeter (15 measurements per load). The squares and the circles are the data points and vertical bars represent one standard deviation. Data-fitted curves are the best fit to data using oxide thickness of 6.4 Å (fibers) and 5.8 Å (shim), Fermi Level 2.0 eV, dielectric constant 4 (see text).

Microsprings

(Ma et al)

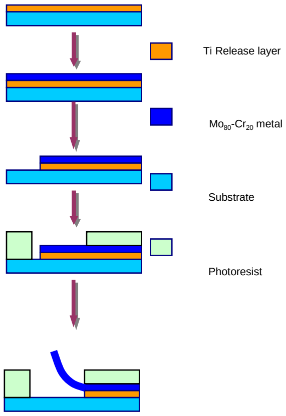

- Sputter deposition: Ti release layer
- Sputter deposition: Mo$_{80}$-Cr$_{20}$ (Stress-engineering)
- Pattern interconnect by photolithography
- Define release window
- Etch release layer
- Interconnect curls up automatically

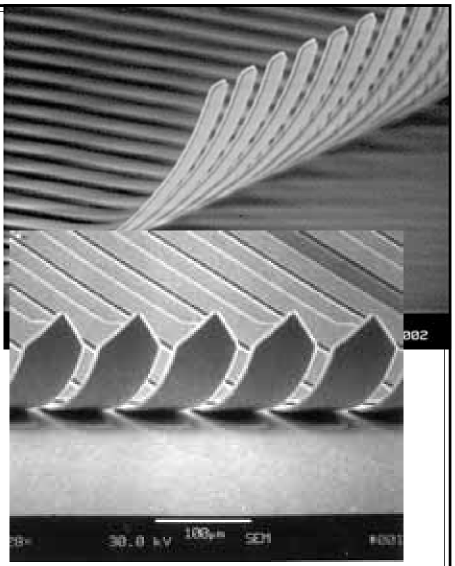

11/13/2009

Nanosprings (Ma et al)

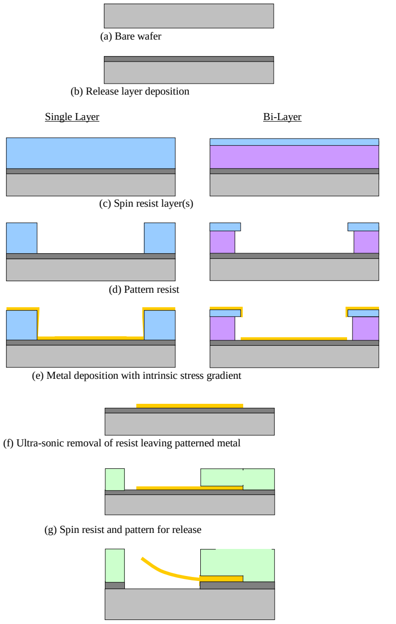

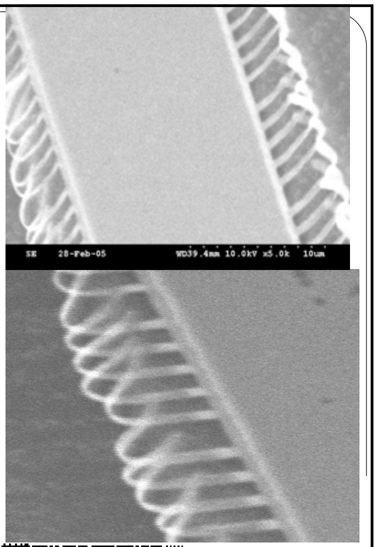

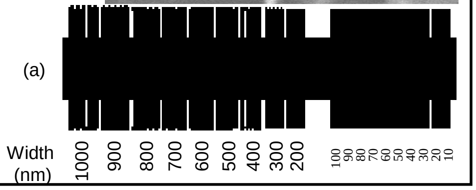

Summary

- Nanopackaging materials (electrical, mechanical, thermal):
  - Nanoparticle applications
  - Carbon nanotube (CNT) applications
  - Electrically conductive adhesives (ECAs)
  - Nanowires, nanospring contacts

- "Nanopackaging: Nanotechnologies in Electronics Packaging," J.E. Morris (editor) Springer (August 2008)
- IEEE Nanotechnology magazine (regular Nanopackaging column)
- IEEE Transactions on Nanotechnology
- Nanotechnology (IOP) www.nanotechweb.org
- IEEE NANO conference (nanopackaging sessions)

Nanoelectronics & Packaging Lab

Portland State
UNIVERSITY